HHS Public Access

Author manuscript

FASEB J. Author manuscript; available in PMC 2022 October 03.

Published in final edited form as:

FASEB J. 2021 June ; 35(6): e21579. doi:10.1096/fj.202002711R.

Preservation of endoplasmic reticulum (ER) Ca^{2+} stores by deletion of inositol-1,4,5-trisphosphate receptor type 1 promotes ER retrotranslocation, proteostasis and protein outer segment localization in cyclic nucleotide-gated channel-deficient cone photoreceptors

Fan Yang,

Hongwei Ma,

Michael R. Butler,

Xi-Qin Ding*

Department of Cell Biology, University of Oklahoma Health Sciences Center, Oklahoma City, Oklahoma

Abstract

Endoplasmic reticulum (ER) Ca^{2+} homeostasis relies on an appropriate balance between efflux- and influx-channel activity responding to dynamic changes of intracellular Ca^{2+} levels. Dysregulation of this complex signaling network has been shown to contribute to neuronal and photoreceptor death in neuro- and retinal degenerative diseases, respectively. In mice with cone cyclic nucleotide-gated (CNG) channel deficiency, a model of achromatopsia/cone dystrophy, cones display early-onset ER stress-associated apoptosis and protein mislocalization. Cones in these mice also show reduced cytosolic Ca^{2+} level and subsequent elevation in the ER Ca^{2+}-efflux-channel activity, specifically the inositol-1,4,5-trisphosphate receptor type 1 (IP_3R1), and deletion of IP_3R1 results in preservation of cones. This work investigated how preservation of ER Ca^{2+} stores leads to cone protection. We examined the effects of cone specific deletion of IP_3R1 on ER stress responses/cone death, protein localization, and ER proteostasis/ER-associated degradation. We demonstrated that deletion of IP_3R1 improves trafficking of cone-specific proteins M-/S-opsin and phosphodiesterase 6C to cone outer segments and reduces localization to cone inner segments. Consistent with the improved protein localization, deletion of IP_3R1 results in increased ER retrotranslocation protein expression, reduced proteasome subunit expression, reduced ER stress/cone death, and reduced retinal remodeling. We also observed the enhanced ER retrotranslocation in mice that have been treated with a chemical chaperone, supporting the connection between improved ER retrotranslocation/proteostasis and alleviation of ER stress. Findings from this work demonstrate the importance of ER Ca^{2+} stores in ER proteostasis and protein trafficking/

*To whom correspondence should be addressed: 940 Stanton L. Young Blvd., BMSB 553, Oklahoma City, Oklahoma 73104, USA; Phone: (405) 271-8001 ext. 47966; Fax: (405) 271-3548; xi-qin-ding@ouhsc.edu.

Author Contribution

FY and HM performed research and analyzed data; FY and XQD designed research and wrote the manuscript. MRB contributed to research design and wrote the manuscript.

All authors declare that they have no conflict of interest.

localization in photoreceptors, strengthen the link between dysregulation of ER Ca^{2+} homeostasis and ER stress/cone degeneration, and support an involvement of improved ER proteostasis in ER Ca^{2+} preservation-induced cone protection; thereby identifying IP_3R1 as a critical mediator of ER stress and protein mislocalization and as a potential target to preserve cones in CNG channel deficiency.

Keywords

Inositol-1,4,5-trisphosphate receptor; ER Ca^{2+} stores; ER stress; CNG channel; cone photoreceptors; retinal degeneration

Introduction

Cone photoreceptor cyclic nucleotide-gated (CNG) channels are essential for phototransduction and cellular Ca^{2+} homeostasis (1). These channels are opened upon binding of cyclic guanosine monophosphate (cGMP) and maintain Ca^{2+} and Na^{+} influx into cone outer segments (OS) (2). Mutations in genes encoding the channel subunits CNGA3 and CNGB3 account for 80% of all cases of achromatopsia and are associated with progressive cone dystrophies (3, 4). These diseases are characterized by severely impaired daylight vision, lack of color discrimination, photophobia, and slow progressing degeneration of cones.

Mice lacking functional cone CNG channels, *Cnga3*$^{-/-}$ and *Cngb3*$^{-/-}$, mimic the phenotype in human patients, displaying early-onset cone degeneration and impaired cone function (5, 6). These mice also show cone opsin mislocalization, i.e., reduced opsin localization to the OS and increased opsin localization to the inner segment (IS) and other photoreceptor regions (5, 6). *Cnga3*$^{-/-}$ and *Cngb3*$^{-/-}$ mice lacking Nrl, a rod-specific neural-retina leucine-zipper transcriptional factor conferring a cone-dominant retina (7), *Cnga3*$^{-/-}$/*Nrl*$^{-/-}$ and *Cngb3*$^{-/-}$/*Nrl*$^{-/-}$, display similar phenotype as that in their respective single knockout lines (8, 9), and thus allow one to examine the cellular and biochemical mechanisms of cone degeneration (cones comprise only 2–3% of the total photoreceptor population in wild-type mouse retina). Studies with these models show that cone death in CNG channel-deficient mice involves endoplasmic reticulum (ER) stress-associated apoptosis (8, 9).

As a non-selective cation channel in the OS of photoreceptors, the CNG channel plays a pivotal role in cellular Ca^{2+} homeostasis. Although permeable to Na^{+} and Ca^{2+}, cone CNG channels have been shown to have higher Ca^{2+} affinity than the channel in rods (10). Thus, cones lacking a functional CNG channel suffer from cellular calcium perturbation/cytoplasmic Ca^{2+} reduction. This has been demonstrated by the measurement of intracellular Ca^{2+} levels using calcium imaging (11). The cytosolic Ca^{2+} reduction in these mice has also been supported by the remarkable elevation in cellular cGMP levels (8, 12), because biosynthesis of cGMP is highly regulated by the Ca^{2+}-guanylate cyclase activating protein-guanylate cyclase (Ca^{2+}-GCAP-GC) axis (13, 14); cytosolic Ca^{2+} level negatively regulates production of cGMP.

Besides cellular Ca^{2+} signaling, ER Ca^{2+} homeostasis plays significant roles in regulating protein folding/trafficking, proteostasis/ER-associated degradation (ERAD), and unfolded protein responses (UPR)/ER stress signaling when these processes are disrupted (15–17). ER Ca^{2+} homeostasis/ER Ca^{2+} stores is primarily regulated by the two ER Ca^{2+} channels, the inositol-1,4,5-trisphosphate receptor (IP_3R) and ryanodine receptor (RyR), for Ca^{2+} efflux out of the ER into the cytosol, and the sarco/endoplasmic reticulum Ca^{2+}-ATPase (SERCA), for Ca^{2+} influx into the ER. ER Ca^{2+} channels are highly regulated by cytosolic Ca^{2+} levels; their activity is increased when cytosolic Ca^{2+} level is low. There are three isoforms of IP_3R: IP_3R1, IP_3R2 and IP_3R3. Transcript expression studies revealed that the levels of IP_3R1 mRNA in the mouse retinas were approximately 6- to 10-fold higher than the expression levels of IP_3R3 mRNA, whereas IP_3R2 mRNA was not detectable in the retinal tissues (11). Consistent with the perturbation of cytosolic Ca^{2+} homeostasis, cones in mice lacking CNG channel show dysregulation of ER Ca^{2+} homeostasis and IP_3R1. Expression/activity of IP_3R1 was significantly increased in CNG channel-deficient retinas (8, 11, 18), likely resulted from decreased cytosolic Ca^{2+} level, as a compensatory effort to increase cytosolic Ca^{2+} level. The potential contribution of ER Ca^{2+} dysregulation/activity of IP_3R1 to cone degeneration was supported by findings in which cone specific deletion of IP_3R1 improved cone survival in *Cnga3*$^{-/-}$ mice (11).

The present study was designed to understand the cellular/molecular mechanisms underlying cone preservation after deletion of IP_3R1. We found that protein localization to cone OS was significantly improved in CNG channel-deficient mice after deletion of IP_3R1 and cone apoptosis was reduced. Correlating with these alterations, deletion of IP_3R1 resulted in significant increase in the expression of ER retrotranslocation proteins, decrease in ER stress responses and downstream death signaling, and decrease in Müller glial cell activity. Similar findings were obtained in mice that have been treated with a chemical chaperone. This work demonstrates the importance of ER Ca^{2+} stores in ER retrotranslocation/proteostasis and protein localization, supports the link between depletion of ER Ca^{2+} stores and ER stress/cone degeneration, and supports a potential involvement of improved ER proteostasis in ER Ca^{2+} store preservation-induced cone protection.

Materials and Methods

The *Cnga3*$^{-/-}$ (5), *Cnga3*$^{-/-}$/*Nrl*$^{-/-}$ (8), *Nrl*$^{-/-}$ (7), *Cnga3*$^{-/-}$/*Itpr1*$^{flox/flox}$/*Hrgp*^{Cre} (11), and *Cnga3*$^{-/-}$/*Nrl*$^{-/-}$/*Ryr2*$^{flox/flox}$/*Hrgp*^{Cre} (19) mouse lines were generated as described previously. The *Cnga3*$^{-/-}$/*Nrl*$^{-/-}$/*Itpr1*$^{flox/flox}$/*Hrgp*^{Cre}, *Nrl*$^{-/-}$/*Itpr1*$^{flox/flox}$/*Hrgp*^{Cre}, and *Itpr1*$^{flox/flox}$/*Hrgp*^{Cre} lines were generated by cross-breeding. The wild-type (C57BL/6J) line was obtained from The Jackson Laboratory (Bar Harbor, ME). All mice were housed under cyclic, 12-h light-dark conditions, with ~7-foot candles of illumination during the light cycle. Animal maintenance and experiments were approved by the local Institutional Animal Care and Use Committee (University of Oklahoma Health Sciences Center, Oklahoma City, OK) and conformed to the guidelines on the care and use of animals accepted by the Society for Neuroscience and the Association for Research in Vision and Ophthalmology (Rockville, MD). Mice of either sex were used in the experiments.

Primary antibody information is listed in Table 1. Biotinylated peanut agglutinin (PNA) was purchased from Vector Laboratories, Inc. (Burlingame, CA, USA). Horseradish peroxidase (HRP)-conjugated anti-rabbit or anti-mouse secondary antibody was obtained from Kirkegaard & Perry Laboratories Inc. (Gaithersburg, MD), fluorescent-conjugated goat anti-rabbit antibody was purchased from Invitrogen (A21428), Streptavidin-Cy3 was purchased from Sigma-Aldrich (S6402), and 4',6-Diamidino-2-phenylindole (DAPI) was purchased from Sigma-Aldrich (D9542). Other reagents were obtained from Sigma, Bio-Rad, Invitrogen, Abcam, and Tocris Biosciences.

Eye preparation, immunofluorescence labeling, and confocal microscopy

Retinal whole mounts or cross sections were prepared for immunofluorescence labeling, as described previously (20). For retinal whole mount preparations, eyes were enucleated, marked at the superior pole with a green dye, and fixed in 4% paraformaldehyde (PFA; Polysciences, Inc., Warrington, PA) for 30 min at room temperature, followed by removal of the cornea and lens. The eyes were then fixed in 4% paraformaldehyde in PBS for 4 – 6 h at room temperature, and retinas were isolated and the superior portion was marked for orientation with a small cut. For retinal cross-sections, mouse eyes were enucleated (the superior portion of the cornea was marked with green dye prior to enucleation) and fixed in Prefer (Anatech Ltd., Battle Creek, MI) for 25–30 min at room temperature. Paraffin sections (5-μm thickness) passing vertically through the retina (along the vertical meridian passing through the optic nerve head) were prepared using a Leica microtome (Leica Biosystems, Buffalo Grove, IL).

Immunofluorescence labeling was performed as described previously (20). Briefly, retinal whole mounts or sections were blocked with Hanks' balanced salt solution containing 5% BSA and 0.5% Triton X-100 for 1 h at room temperature or overnight at 4°C. Prior to blocking, antigen retrieval was performed in 10 mM sodium citrate buffer (pH 6.0) in a 70°C water bath. Primary-antibody incubation was performed for 2 h at room temperature or overnight at 4°C (see Table 1 for antibody information). Slides were mounted and coverslipped after fluorescence-conjugated secondary-antibody incubation and wash steps. Immunofluorescence labeling was then imaged using an Olympus FV1000 confocal laser-scanning microscope and FluoView imaging software (Olympus, Melville, NY). For evaluations of cone OS protein cellular localization, confocal images of 10 layers were stacked with the Z-stack function in the ImageJ software (https://imagej.nih.gov/ij/) to obtain a maximal immunofluorescence density. Fluorescence density levels of the immunolabeling in the OS, IS, outer nuclear layer (ONL), and outer plexiform layer (OPL) were measured, and the density levels at each region relative to the total fluorescence density were calculated and averaged from at least three sections per eye from at least five animals per condition.

TUNEL assay

Terminal deoxynucleotidyl transferase dUTP nick-end labeling (TUNEL) was performed to analyze photoreceptor apoptotic death as described previously (18), using paraffin-embedded retinal sections and an *in situ* cell death fluorescein detection kit (Roche Applied Science, Ref. 11684795910). Immunofluorescence labeling was imaged using an Olympus

FV1000 confocal laser-scanning microscope, and TUNEL-positive cells in the ONL passing through the optic nerve were counted and averaged from at least three sections per eye from at least four animals per condition.

Retinal protein preparation, SDS-PAGE, and western blot analysis

Retinal protein preparation, SDS-PAGE, and western blot analysis were performed as described previously (18). Briefly, retinas were homogenized in homogenization buffer A [0.32 M sucrose, 20 mM 4-(2-hydroxyethyl)-1-piperazineethanesulfonic acid (HEPES), pH 7.4, and 3 mM EDTA containing protease and phosphatase inhibitors] (Roche Applied Science, catalog no. 04693159001 and 04906837001, respectively), and homogenates were centrifuged at 1,200 g for 10 min at 4°C. The resulting supernatant was then centrifuged at 21,000 g for 35 min at 4°C to separate cytosolic (supernatant) and membrane (pellet) fractions. The resulting membrane pellet was resuspended in homogenization buffer B [0.32 M sucrose, 20 mM HEPES, pH 7.4, 3 mM EDTA, and 0.1% Triton X-100 containing protease and phosphatase inhibitors], sonicated twice for 15 s on ice at a medium speed using an XL2000 Ultrasonic Cell Disruptor (Misonix, Farmingdale, NY, USA), with a 30-s recovery between disruptions, and incubated for 1 h at 4°C with gentle agitation. After incubation, the homogenate was centrifuged at 21,000 g for 35 min at 4°C, and the resulting supernatant was used as the membrane fraction. All protein concentrations were determined by a protein-assay kit from Bio-Rad Laboratories. Retinal protein samples (20 μg protein per sample) were then subjected to SDS-PAGE and transferred to PVDF membranes, followed by blocking in 5% bovine serum albumin (BSA) for 1 h at room temperature. Immunoblots were incubated with primary antibody overnight at 4°C. After washing in Tris-buffered saline with 0.1% Tween 20, immunoblots were incubated with horseradish peroxidase-conjugated secondary antibody (1:20,000) for 1 h at room temperature. SuperSignal® West Dura Extended Duration chemiluminescent substrate (Thermo Fisher Scientific, catalog no. 34076) was used to detect binding of the primary antibodies to their cognate antigens. An Li-Cor Odyssey CLx Imager and Li-Cor software (Li-Cor Biosciences, Lincoln, NE, USA) were used for detection and densitometric analysis.

PCR array

Total RNA preparation and reverse transcription were performed as described previously (9). The Mouse Unfolded Protein Response RT^2 Profiler PCR Array (Qiagen, Hiden, Germany), which profiles the expression of 84 genes involved in unfolded protein binding, protein folding, endoplasmic-reticulum-associated protein degradation, and heat shock proteins, was used under the manufacturer's instructions.

TUDCA treatment

Treatment of *Cnga3*$^{-/-}$/*Nrl*$^{-/-}$ mice with tauroursodeoxycholic acid (TUDCA) was performed as described previously (9, 21). Briefly, TUDCA (500 mg/kg, body weight, TCI America) or vehicle (0.15 M $NaHCO_3$, pH 7.0) was given to *Cnga3*$^{-/-}$/*Nrl*$^{-/-}$ mice by subcutaneous injection every 3 days for 12 days, starting at P5. Retinas were collected at the end of the treatment for western blotting analysis.

Statistical analysis

One-way analysis of variance and unpaired Student's *t* test were used to evaluate significant differences between multiple groups and two groups, respectively. Statistical analyses and graph generation were performed using GraphPad Prism® software (GraphPad Software, San Diego) for Windows.

Results

Deletion of IP_3R1 reduces ER stress, downstream death signaling, and cone apoptosis in CNG channel-deficient retinas.

To demonstrate the contribution of IP_3R1 activity to ER stress, we evaluated the effects of cone-specific deletion of IP_3R1. Mouse retinas at postnatal day 15 (P15) and P30 were analyzed for ER stress markers by immunoblotting. As shown in Figure 1A, $Cnga3^{-/-}/Nrl^{-/-}/Itpr1^{flox/flox}/Hrgp^{Cre}$ retinas showed significantly reduced phospho-eukaryotic-initiation factor 2α (p-eIF2α) levels at P15 and P30 when compared to age-matched $Cnga3^{-/-}/Nrl^{-/-}$ controls, approaching the baseline level found in the age-matched control $Nrl^{-/-}/Itpr1^{flox/flox}/Hrgp^{Cre}$ mice (the expression level in $Nrl^{-/-}/Itpr1^{flox/flox}/Hrgp^{Cre}$ retina was not different from that in $Nrl^{-/-}$ retina, data not shown). In addition, phospho-serine/threonine-protein kinase/endoribonuclease 1α (p-IRE1α) level was significantly reduced in $Cnga3^{-/-}/Nrl^{-/-}/Itpr1^{flox/flox}/Hrgp^{Cre}$ retinas at P30 when compared to age-matched $Cnga3^{-/-}/Nrl^{-/-}$ controls, and also approach baseline level (Fig. 1A). Furthermore, we analyzed the effects of IP_3R1 deletion on transcriptional regulation of ER stress signaling, and found nearly complete return to baseline mRNA expression levels of each marker tested (Fig. 1B). These results suggest that reducing IP_3R1 activity attenuates ER-stress responses at both transcriptional and translational levels in CNG channel-deficient retinas.

The effects of IP_3R1 deletion were further examined by evaluating the expression of CHOP, a member of the C/EBP (CCAAT enhancer-binding protein) transcription factor family induced in ER stress (22) and involved in ER stress-associated apoptosis (23, 24). We have previously shown increased expression/activation of CHOP in CNG channel-deficient retina (8). Nuclear protein preparations from mouse retina at P15 were analyzed for CHOP expression. The analysis showed that deletion of IP_3R1 completely abolished CHOP activation in $Cnga3^{-/-}/Nrl^{-/-}/Itpr1^{flox/flox}/Hrgp^{Cre}$ retinas (Fig. 2A).

The basic/leucine zipper transcription factor Creb (cyclic adenosine monophosphate response element binding protein) is activated by UPR/ER stress signaling (25). We have shown increased expression/activation of Creb signaling in CNG channel-deficient retina (26). In the present study, we evaluated whether deletion of IP_3R1 affects Creb signaling. Nuclear protein preparations from mouse retina at P30 were analyzed for Creb expression/activity. The analysis showed that the phospho-Creb level was increased by about 50% in $Cnga3^{-/-}/Nrl^{-/-}$ mice, compared with $Nrl^{-/-}$ retinas, and deletion of IP_3R1 abolished this elevation (Fig. 2B).

To confirm the contribution of IP_3R1 activity to cone apoptosis, we evaluated whether deletion of IP_3R1 reduces apoptotic cone death by TUNEL. The analysis revealed that

the retinal sections of *Cnga3*$^{-/-}$/*Itpr1*$^{flox/flox}$/*Hrgp*^{Cre} mice and *Cnga3*$^{-/-}$/*Nrl*$^{-/-}$/*Itpr1*$^{flox/flox}$/*Hrgp*^{Cre} mice at P15 display a significant reduction in the number of TUNEL-positive cells when compared with their respective age-matched controls (Fig. 2C).

Deletion of IP_3R1 increases cone survival and reduces Müller glial cell activation in CNG channel-deficient retinas.

In addition, we analyzed PNA-labeled retinal sections to evaluate cone survival in these mice at 2 months and found improved survival after IP_3R1 deletion (Fig. 3A). Improved cone survival was also shown by increased expression level of M-opsin in *Cnga3*$^{-/-}$/*Nrl*$^{-/-}$/*Itpr1*$^{flox/flox}$/*Hrgp*^{Cre} mice, compared with *Cnga3*$^{-/-}$/*Nrl*$^{-/-}$ mice (Fig. 3B).

Increased Müller glial cell activity is associated with retinal degeneration and is commonly assessed by glial fibrillary acidic protein (GFAP) immunolabeling (27–29). Increased GFAP activity has been documented in retinas of *Cnga3*$^{-/-}$ and *Cnga3*$^{-/-}$/*Nrl*$^{-/-}$ mice (18, 19, 30) as a consequence of progressive cone degeneration. We examined GFAP expression in CNG channel-deficient mice at P30 after deletion of IP_3R1. The results in Figure 4 show reduced GFAP immunofluorescence to near baseline in *Cnga3*$^{-/-}$/*Itpr1*$^{flox/flox}$/*Hrgp*^{Cre} retinal sections when compared to age-matched *Cnga3*$^{-/-}$ mice (Fig. 4A). We also measured GFAP protein levels in these mice using immunoblotting and similar trends were obtained (Fig. 4B).

Deletion of IP_3R1 improves cone opsin localization to OS in CNG channel-deficient cones.

To evaluate the contributions of IP_3R1 activity to cone opsin mislocalization, we examined the effects of IP_3R1 deletion. As shown in Figure 5A, M-opsin localization to cone OS was significantly increased in *Cnga3*$^{-/-}$/*Itpr1*$^{flox/flox}$/*Hrgp*^{Cre} mice at 4 months (from 17–31% in *Cnga3*$^{-/-}$ mice to 30–40% in *Cnga3*$^{-/-}$/*Itpr1*$^{flox/flox}$/*Hrgp*^{Cre} mice). Furthermore, M-opsin levels were significantly decreased in cone IS in *Cnga3*$^{-/-}$/*Itpr1*$^{flox/flox}$/*Hrgp*^{Cre} mice, providing additional evidence for improved M-opsin trafficking (Fig. 5A). Similar findings were obtained with S-opsin labeling. Deletion of IP_3R1 significantly improved S-opsin localization to cone OS and reduced S-opsin mislocalization to cone IS, ONL, and OPL when compared to age-matched *Cnga3*$^{-/-}$ controls (Fig. 5B).

Deletion of IP_3R1 improves PDE6C localization to OS in CNG channel-deficient cones.

To gain additional evidence for the contribution of IP_3R1 activity to cone protein mislocalization, we analyzed the effects of IP_3R1 deletion on the trafficking of another cone-specific protein, the phosphodiesterase 6C (PDE6C). The data in Figure 6 show that *Cnga3*$^{-/-}$/*Itpr1*$^{flox/flox}$/*Hrgp*^{Cre} retinas have improved PDE6C localization to cone OS when compared to age-matched *Cnga3*$^{-/-}$ controls (Fig. 6). Together with the opsin localization data, these results indicate IP_3R1 activity contributes to impairment of global protein trafficking found in CNG channel deficiency and deletion of IP_3R1 improves protein trafficking.

Deletion of IP_3R1 increases expression of ER retrotranslocation proteins in CNG channel-deficient retinas.

ER protein retrotranslocation and the subsequent ubiquitination-mediated degradation *via* proteasomes is a critical mechanism to maintain ER proteostasis/ER function and regulate UPR/ER stress. ER retrotranslocation is a process involving multiple machinery proteins, including Syvn1 (E3 ubiquitin-protein ligase synoviolin 1, directing ubiquitination and targeting to proteasomes for degradation) (31, 32), Sel1L (ERAD E3 ligase adaptor subunit) (33, 34), Herpud1 (homocysteine inducible ER protein with ubiquitin like domain 1) (35, 36), and Derlin-1 (degradation in ER protein 1) (37, 38). We examined expression of these proteins in CNG channel-deficient retina at P15 and P30, and the effects of IP_3R1 deletion. We found that the expression levels of Syvn1, Sel1L, and Herpud1 were unchanged in $Cnga3^{-/-}/Nrl^{-/-}$ mice, compared with $Nrl^{-/-}$ controls. However, deletion of IP_3R1 significantly increased expression of these proteins (Fig. 7A). Interestingly, expression of Derlin-1 was increased in CNG channel-deficient retina and deletion of IP_3R1 completely abolished this upregulation (Fig. 7B). To assess whether these observations are associated with ER Ca^{2+} stores but not the IP_3R1 channel itself, we included a second mouse line with deletion of RyR2 ($Cnga3^{-/-}/Nrl^{-/-}/Ryr2^{flox/flox}/Hrgp^{Cre}$) and obtained similar findings (Fig. 7A). In a separate experiment, we examined whether a chemical chaperone that reduces ER stress also increases expression of the ER retrotranslocation proteins. We treated $Cnga3^{-/-}/Nrl^{-/-}$ mice with TUDCA, a well-known chemical chaperone that has been proven to reduce ER stress and photoreceptor cell death (21, 39, 40), including ER stress/cone death in $Cnga3^{-/-}/Nrl^{-/-}$ retinas (9, 11). Immunoblotting analysis showed that expression levels of Syvn1, Sel1L, and Herpud1 were significantly increased after TUDCA treatment, compared with vehicle-treated controls. However, TUDCA treatment did not alter the expression of Derlin-1 (Fig. 7C).

Deletion of IP_3R1 decreases expression of the proteasome subunit in CNG channel-deficient retinas.

We extended our evaluations to expression of the proteasome machinery. The proteasome subunits proteasome activator 28α (PA28α) and PA28β form a heteroheptameric complex and function by binding to the 20S proteasome complex (41), whereas PSMD11 (proteasome 26S subunit, non-ATPase 1) is a component of the 19S regulator of the proteasomes. We examined expression of PA28α and PSMD11 in CNG channel-deficient retinas after deletion of IP_3R1. We found that the expression levels of PA28α was not different between $Cnga3^{-/-}/Nrl^{-/-}$ and age-matched $Nrl^{-/-}$ retinas. However, deletion of IP_3R1 or RyR2 significantly reduced expression levels of PA28α in CNG channel-deficient retinas, and this reduction was observed at P15 but not P30 (Fig. 8A). In contrast to changes in PA28α, expression levels of PSMD11 remained unchanged among the different genotypes (Fig. 8A). Similar to findings in mice with IP_3R1 deletion, PA28α expression level was significantly reduced after TUDCA treatment whereas PSMD11 remained unchanged (Fig. 8B).

Deletion of IP_3R1 does not affect autophagy activity in CNG channel-deficient retinas.

It has been known that UPR/ER stress induces/increases autophagy (42, 43). We examined markers for autophagy in CNG channel-deficient retinas and the effects of IP_3R1 deletion. As shown in Figure 9, the expression levels of SQSTM1/p62 and LC3B II were significantly elevated in *Cnga3*$^{-/-}$/*Nrl*$^{-/-}$ retinas. However, deletion of IP_3R1 or RyR2 did not induce further alterations (Fig. 9A). Similar findings were observed in TUDCA-treated *Cnga3*$^{-/-}$/*Nrl*$^{-/-}$ retinas. Expression levels of SQSTM1/p62 and LC3B II remained the same in mice with and without TUDCA treatment (Fig. 9B).

Discussion

In our previous work, we have documented ER stress-associated apoptotic cone death and protein mislocalization in CNG channel-deficient mice. Retinas of these mice show elevation of all three arms of the ER stress pathways, i.e., elevated levels of phospho-eIF2α and phospho-IRE1α and increased cleavage of ATF6 (8, 11, 18), as well as increased nuclear localization of CHOP (8, 18). CNG channel-deficient cones also show reduced cytosolic Ca^{2+} levels at early ages and a subsequent increase in the expression/activity of IP_3R1 (11). Furthermore, pharmacological inhibition of IP_3R using chemical inhibitors significantly reduces ER stress/cone death and improves protein OS localization, and deletion of IP_3R1 improved cone survival (11). The present study expanded on the previous work and explored the mechanism(s) underlying how deletion of IP_3R1 leads to cone protection. Based on the known connections between ER Ca^{2+} dysregulation and ER stress (44) and our previous findings, we hypothesized that IP_3R1 deletion would preserve ER Ca^{2+} stores/improve ER Ca^{2+} homeostasis, resulting in improved protein trafficking/proteostasis and subsequent reduction in ER stress. Consistent with our predictions, the present work demonstrated improved localization of M-/S-opsin and PDE6C to cone OS and reduced localization to cone IS after deletion of IP_3R1, reduced ER stress responses/cone apoptosis, reduced Müller glial cell activation, and early-onset cone protection. Moreover, deletion of IP_3R1 increased expression of the ER retrotranslocation proteins and reduced expression of the proteasome proteins, suggesting that the protective effects of IP_3R1 deletion may be related to a potentially improved ER proteostasis. Thus, targeting IP_3R1 is sufficient to rebalance ER Ca^{2+} homeostasis in CNG channel deficiency, improve ER proteostasis, and reduce ER stress/cone apoptosis, representing a novel strategy for cone protection.

The potential mechanism underlying improved protein trafficking/OS localization and reduced ER stress after IP_3R1 deletion may involve an increased ER retrotranslocation/improved proteostasis. The expression levels of the retrotranslocation complex proteins Syvn 1, Sel1L and Herpud1 were significantly increased after IP_3R1 deletion. Similar findings were observed in mice that have been treated with TUDCA. Increased ER retrotranslocation would relieve ER protein accumulation and facilitate the degradation of some death signaling molecules. Syvn1 is known to reduce ER stress-associated apoptosis through increased clearance of IRE1α and CHOP (45, 46). Consistent with this finding, the present work show reduced levels of phospho-IRE1α and CHOP after IP_3R1 deletion. We presume that deletion of IP_3R1 improves ER protein retrotranslocation/ER

proteostasis, which in turn reduces ER stress/cone death and improves protein trafficking/cone survival. Furthermore, the reduction in ER stress activity including improved protein folding/trafficking globally may subsequently reduce proteasome activity because of a decreased demand for protein clearance. This prediction was supported by the reduction of the proteasome component PA28α. Previous studies have shown upregulation of the proteasome components in retinal degeneration resulting from misfolding mutations in rhodopsin (P23H mutation) (47), and proteasome overload has been implicated as a mechanism of photoreceptor death (48). Nevertheless, our findings suggest that preservation of ER Ca^{2+} stores is sufficient to improve ER proteostasis and reduce ER stress and the subsequent proteasome burden. Although the intermediate signaling connecting ER Ca^{2+} stores with ER retrotranslocation machinery and proteasome capacity requires further exploration, enhancing ER retrotranslocation may represent a potential approach to improve ER proteostasis/relieve ER stress in retinal degeneration. Indeed, over expression of Syvn1 has been shown to reduce retinal degeneration in diabetic retinopathy (49).

ER stress and ER stress-associated apoptotic cone death is an early event in CNG channel deficiency (8, 18). The present study showed that the reduction in phospho-IRE1α and phospho-eIF2α was observed as early as P15 after IP_3R1 deletion, supporting a decrease in ER stress at early age. Furthermore, cone preservation/increased cone density was already apparent at 2 months. When combined with previous results showing improved cone density at older ages (4 and 8 months) (11), our findings suggest that early intervention to reduce ER stress in CNG-channel deficiency can lead to early-onset, sustained cone preservation.

Although ER stress responses were nearly completely reversed in CNG channel-deficient mice after deletion of IP_3R1 and cone apoptosis was greatly reduced, protein localization and cone density were only partially improved/resumed. These observations suggest that the stabilization of ER Ca^{2+} stores was likely incomplete. The contributions of other ER Ca^{2+} channels, like RyR2, cannot be overlooked due to their up-regulation in CNG channel deficiency and the contribution to protein mislocalization and ER stress, as shown previously (11, 19). It can be predicted that deletion of both IP_3R1 and RyR2 would enhance the improvement of protein trafficking and cone survival. The IS membrane Ca^{2+} channels, such as stromal interaction molecule (STIM) proteins and transient receptor potential channels (TRPCs) (50, 51), may contribute to disruption of ER Ca^{2+} homeostasis in the channel-deficient mice. In addition, cone OS malformation is a hallmark of CNG channel deficiency (5, 52) and presents a persistent mechanical barrier to protein transport.

Autophagy activity was elevated in CNG channel-deficient retina. However, deletion of IP_3R1 did not suppress activation of autophagy. This finding suggests that preservation of ER Ca^{2+} store may not be sufficient enough to correct autophagy in CNG channel deficiency. It may also suggest that autophagy in CNG channel deficiency does not primarily involve an ER stress-related mechanism although ER stress has been shown to induce autophagy (53). The sustained elevation of autophagy activity after IP_3R1 deletion may contribute in part to the partial rescue of cone survival/density.

In summary, the present study demonstrates that IP_3R1 deletion improves cone protein trafficking to OS and reduces ER stress/apoptosis, leading to cone preservation. The

improved ER retrotranslocation/proteostasis after deletion of IP_3R1 may underlie the observed cone protection. Findings from the present work identify IP_3R1 activity as a key mediator of dysfunctional ER Ca^{2+} homeostasis and subsequent ER stress, protein mislocalization, and cone death in CNG channel deficiency, revealing a novel mechanism of photoreceptor degeneration. Importantly, these results support early intervention to stabilize cone Ca^{2+} dynamics and that doing so leads to improvement in photoreceptor viability. Altered Ca^{2+} signaling, ER stress, and dysfunctional proteostasis are common phenotypes of many different types of retinal degenerative diseases. Understanding the molecular components contributing to these disease-promoting processes will help develop novel strategies to stabilize cytosolic-ER Ca^{2+} dynamics and slow photoreceptor death in retinal degeneration.

Acknowledgments

We thank Drs. Martin Biel, Anand Swaroop, Katsuhiko Mikoshiba, and Yun-Zheng Le for providing *Cnga3*$^{-/-}$, *Nrl*$^{-/-}$, *Itpr1*$^{flox/flox}$, and *Hrgp*^{cre} mouse lines. We thank the Histology, Microscopy, and Image Analysis Core Facility at OUHSC for technical assistance.

This work was supported by grants from the National Eye Institute (R01EY027754 and P30EY021725) and the Oklahoma Center for the Advancement of Science and Technology.

Abbreviations used:

cGMP	cyclic guanosine monophosphate
CHOP	CCAAT-enhancer-binding protein homologous protein
CNG	cyclic nucleotide-gated
Creb	cyclic adenosine monophosphate response element binding protein
Derlin-1	degradation in ER protein 1
ER	endoplasmic reticulum
eIF2α	eukaryotic translation initiation factor 2 alpha
ERAD	ER-associated degradation
GFAP	glial fibrillary acidic protein
Herpud1	homocysteine inducible ER protein with ubiquitin like domain 1
HRGP	human red/green pigment
IP_3R 1	inositol-1,4,5-trisphosphate receptor type 1
Ire1α	serine/threonine-protein kinase/endoribonuclease 1α
LC3B	microtubule-associated proteins 1A/1B light chain 3B
PA28α	proteasome activator complex subunit 1

PDE	phosphodiesterase
PNA	peanut agglutinin lectin
PSMD11	26S proteasome non-ATPase regulatory subunit 11
qRT-PCR	quantitative reverse transcription polymerase chain reaction
RyR2	ryanodine receptor type 2
Sel1L	ERAD E3 ligase adaptor subunit
SQSTM1/P62	sequestosome-1
Syvn1	E3 ubiquitin-protein ligase synoviolin 1
TBP	TATA binding protein
TUDCA	tauroursodeoxycholic acid
TUNEL	terminal deoxynucleotidyl transferase dUTP nick end-labeling
UPR	unfolded protein response

References

1. Kaupp UB, and Seifert R (2002) Cyclic nucleotide-gated ion channels. Physiol Rev 82, 769–824 [PubMed: 12087135]
2. Kohl S, Baumann B, Broghammer M, Jagle H, Sieving P, Kellner U, Spegal R, Anastasi M, Zrenner E, Sharpe LT, and Wissinger B (2000) Mutations in the CNGB3 gene encoding the beta-subunit of the cone photoreceptor cGMP-gated channel are responsible for achromatopsia (ACHM3) linked to chromosome 8q21. Hum Mol Genet 9, 2107–2116 [PubMed: 10958649]
3. Kohl S, Marx T, Giddings I, Jagle H, Jacobson SG, Apfelstedt-Sylla E, Zrenner E, Sharpe LT, and Wissinger B (1998) Total colourblindness is caused by mutations in the gene encoding the alpha-subunit of the cone photoreceptor cGMP-gated cation channel. Nat Genet 19, 257–259 [PubMed: 9662398]
4. Nishiguchi KM, Sandberg MA, Gorji N, Berson EL, and Dryja TP (2005) Cone cGMP-gated channel mutations and clinical findings in patients with achromatopsia, macular degeneration, and other hereditary cone diseases. Hum Mutat 25, 248–258 [PubMed: 15712225]
5. Biel M, Seeliger M, Pfeifer A, Kohler K, Gerstner A, Ludwig A, Jaissle G, Fauser S, Zrenner E, and Hofmann F (1999) Selective loss of cone function in mice lacking the cyclic nucleotide-gated channel CNG3. Proc Natl Acad Sci U S A 96, 7553–7557 [PubMed: 10377453]
6. Xu J, Morris L, Fliesler SJ, Sherry DM, and Ding XQ (2011) Early-onset, slow progression of cone photoreceptor dysfunction and degeneration in CNG channel subunit CNGB3 deficiency. Invest Ophthalmol Vis Sci 52, 3557–3566 [PubMed: 21273547]
7. Mears AJ, Kondo M, Swain PK, Takada Y, Bush RA, Saunders TL, Sieving PA, and Swaroop A (2001) Nrl is required for rod photoreceptor development. Nat Genet 29, 447–452 [PubMed: 11694879]
8. Thapa A, Morris L, Xu J, Ma H, Michalakis S, Biel M, and Ding XQ (2012) Endoplasmic reticulum stress-associated cone photoreceptor degeneration in cyclic nucleotide-gated channel deficiency. J Biol Chem 287, 18018–18029 [PubMed: 22493484]
9. Ma H, Thapa A, Morris LM, Michalakis S, Biel M, Frank MB, Bebak M, and Ding XQ (2013) Loss of cone cyclic nucleotide-gated channel leads to alterations in light response modulating system

and cellular stress response pathways: a gene expression profiling study. Hum Mol Genet 22, 3906–3919 [PubMed: 23740940]

10. Hackos DH, and Korenbrot JI (1999) Divalent cation selectivity is a function of gating in native and recombinant cyclic nucleotide-gated ion channels from retinal photoreceptors. J Gen Physiol 113, 799–818 [PubMed: 10352032]
11. Butler MR, Ma H, Yang F, Belcher J, Le YZ, Mikoshiba K, Biel M, Michalakis S, Iuso A, Krizaj D, and Ding XQ (2017) Endoplasmic reticulum (ER) Ca(2+)-channel activity contributes to ER stress and cone death in cyclic nucleotide-gated channel deficiency. J Biol Chem 292, 11189–11205 [PubMed: 28495882]
12. Xu J, Morris L, Thapa A, Ma H, Michalakis S, Biel M, Baehr W, Peshenko IV, Dizhoor AM, and Ding XQ (2013) cGMP accumulation causes photoreceptor degeneration in CNG channel deficiency: evidence of cGMP cytotoxicity independently of enhanced CNG channel function. J Neurosci 33, 14939–14948 [PubMed: 24027293]
13. Olshevskaya EV, Ermilov AN, and Dizhoor AM (2002) Factors that affect regulation of cGMP synthesis in vertebrate photoreceptors and their genetic link to human retinal degeneration. Mol Cell Biochem 230, 139–147 [PubMed: 11952089]
14. Baehr W, and Palczewski K (2009) Focus on Molecules: Guanylate cyclase-activating proteins (GCAPs). Experimental Eye Research 89, 2–3 [PubMed: 19162008]
15. Gorlach A, Klappa P, and Kietzmann T (2006) The endoplasmic reticulum: folding, calcium homeostasis, signaling, and redox control. Antioxidants & redox signaling 8, 1391–1418 [PubMed: 16986999]
16. Mekahli D, Bultynck G, Parys JB, De Smedt H, and Missiaen L (2011) Endoplasmic-reticulum calcium depletion and disease. Cold Spring Harb Perspect Biol 3
17. Sammels E, Parys JB, Missiaen L, De Smedt H, and Bultynck G (2010) Intracellular Ca2+ storage in health and disease: a dynamic equilibrium. Cell Calcium 47, 297–314 [PubMed: 20189643]
18. Ma H, Butler MR, Thapa A, Belcher J, Yang F, Baehr W, Biel M, Michalakis S, and Ding XQ (2015) cGMP/Protein Kinase G Signaling Suppresses Inositol 1,4,5-Trisphosphate Receptor Phosphorylation and Promotes Endoplasmic Reticulum Stress in Photoreceptors of Cyclic Nucleotide-gated Channel-deficient Mice. J Biol Chem 290, 20880–20892 [PubMed: 26124274]
19. Ma H, Yang F, Butler MR, Rapp J, Le YZ, and Ding XQ (2019) Ryanodine Receptor 2 Contributes to Impaired Protein Localization in Cyclic Nucleotide-Gated Channel Deficiency. eNeuro 6
20. Ma H, Thapa A, Morris L, Redmond TM, Baehr W, and Ding XQ (2014) Suppressing thyroid hormone signaling preserves cone photoreceptors in mouse models of retinal degeneration. Proc Natl Acad Sci U S A 111, 3602–3607 [PubMed: 24550448]
21. Zhang T, Baehr W, and Fu Y (2012) Chemical chaperone TUDCA preserves cone photoreceptors in a mouse model of Leber congenital amaurosis. Invest Ophthalmol Vis Sci 53, 3349–3356 [PubMed: 22531707]
22. Li J, Lee B, and Lee AS (2006) Endoplasmic reticulum stress-induced apoptosis: multiple pathways and activation of p53-up-regulated modulator of apoptosis (PUMA) and NOXA by p53. J Biol Chem 281, 7260–7270 [PubMed: 16407291]
23. Szegezdi E, Logue SE, Gorman AM, and Samali A (2006) Mediators of endoplasmic reticulum stress-induced apoptosis. EMBO Rep 7, 880–885 [PubMed: 16953201]
24. Nishitoh H (2012) CHOP is a multifunctional transcription factor in the ER stress response. J Biochem 151, 217–219 [PubMed: 22210905]
25. Kikuchi D, Tanimoto K, and Nakayama K (2016) CREB is activated by ER stress and modulates the unfolded protein response by regulating the expression of IRE1alpha and PERK. Biochem Biophys Res Commun 469, 243–250 [PubMed: 26642955]
26. Yang F, Ma H, Butler MR, and Ding XQ (2020) Potential contribution of ryanodine receptor 2 upregulation to cGMP/PKG signaling-induced cone degeneration in cyclic nucleotide-gated channel deficiency. FASEB J 34, 6335–6350 [PubMed: 32173907]
27. de Raad S, Szczesny PJ, Munz K, and Reme CE (1996) Light damage in the rat retina: glial fibrillary acidic protein accumulates in Muller cells in correlation with photoreceptor damage. Ophthalmic Res 28, 99–107 [PubMed: 8792360]

28. Bringmann A, and Reichenbach A (2001) Role of Muller cells in retinal degenerations. Front Biosci 6, E72–92 [PubMed: 11578954]
29. Zhao TT, Tian CY, and Yin ZQ (2010) Activation of Muller cells occurs during retinal degeneration in RCS rats. Adv Exp Med Biol 664, 575–583 [PubMed: 20238061]
30. Michalakis S, Geiger H, Haverkamp S, Hofmann F, Gerstner A, and Biel M (2005) Impaired opsin targeting and cone photoreceptor migration in the retina of mice lacking the cyclic nucleotide-gated channel CNGA3. Invest Ophthalmol Vis Sci 46, 1516–1524 [PubMed: 15790924]
31. Carvalho P, Stanley AM, and Rapoport TA (2010) Retrotranslocation of a misfolded luminal ER protein by the ubiquitin-ligase Hrd1p. Cell 143, 579–591 [PubMed: 21074049]
32. Kaneko M, Ishiguro M, Niinuma Y, Uesugi M, and Nomura Y (2002) Human HRD1 protects against ER stress-induced apoptosis through ER-associated degradation. FEBS Lett 532, 147–152 [PubMed: 12459480]
33. Sun S, Shi G, Han X, Francisco AB, Ji Y, Mendonca N, Liu X, Locasale JW, Simpson KW, Duhamel GE, Kersten S, Yates JR 3rd, Long Q, and Qi L (2014) Sel1L is indispensable for mammalian endoplasmic reticulum-associated degradation, endoplasmic reticulum homeostasis, and survival. Proc Natl Acad Sci U S A 111, E582–591 [PubMed: 24453213]
34. Kaneko M, Yasui S, Niinuma Y, Arai K, Omura T, Okuma Y, and Nomura Y (2007) A different pathway in the endoplasmic reticulum stress-induced expression of human HRD1 and SEL1 genes. FEBS Lett 581, 5355–5360 [PubMed: 17967421]
35. Huang CH, Chu YR, Ye Y, and Chen X (2014) Role of HERP and a HERP-related protein in HRD1-dependent protein degradation at the endoplasmic reticulum. J Biol Chem 289, 4444–4454 [PubMed: 24366871]
36. Paredes F, Parra V, Torrealba N, Navarro-Marquez M, Gatica D, Bravo-Sagua R, Troncoso R, Pennanen C, Quiroga C, Chiong M, Caesar C, Taylor WR, Molgo J, San Martin A, Jaimovich E, and Lavandero S (2016) HERPUD1 protects against oxidative stress-induced apoptosis through downregulation of the inositol 1,4,5-trisphosphate receptor. Free Radic Biol Med 90, 206–218 [PubMed: 26616647]
37. Kadowaki H, Satrimafitrah P, Takami Y, and Nishitoh H (2018) Molecular mechanism of ER stress-induced pre-emptive quality control involving association of the translocon, Derlin-1, and HRD1. Sci Rep 8, 7317 [PubMed: 29743537]
38. Ye Y, Shibata Y, Yun C, Ron D, and Rapoport TA (2004) A membrane protein complex mediates retro-translocation from the ER lumen into the cytosol. Nature 429, 841–847 [PubMed: 15215856]
39. Mantopoulos D, Murakami Y, Comander J, Thanos A, Roh M, Miller JW, and Vavvas DG (2011) Tauroursodeoxycholic acid (TUDCA) protects photoreceptors from cell death after experimental retinal detachment. PLoS One 6, e24245 [PubMed: 21961034]
40. Fernandez-Sanchez L, Lax P, Pinilla I, Martin-Nieto J, and Cuenca N (2011) Tauroursodeoxycholic acid prevents retinal degeneration in transgenic P23H rats. Invest Ophthalmol Vis Sci 52, 4998–5008 [PubMed: 21508111]
41. Song X, von Kampen J, Slaughter CA, and DeMartino GN (1997) Relative functions of the alpha and beta subunits of the proteasome activator, PA28. J Biol Chem 272, 27994–28000 [PubMed: 9346951]
42. Smith M, and Wilkinson S (2017) ER homeostasis and autophagy. Essays Biochem 61, 625–635 [PubMed: 29233873]
43. Qi Z, and Chen L (2019) Endoplasmic Reticulum Stress and Autophagy. Adv Exp Med Biol 1206, 167–177 [PubMed: 31776985]
44. Krebs J, Agellon LB, and Michalak M (2015) Ca(2+) homeostasis and endoplasmic reticulum (ER) stress: An integrated view of calcium signaling. Biochem Biophys Res Commun 460, 114–121 [PubMed: 25998740]
45. Gao B, Lee SM, Chen A, Zhang J, Zhang DD, Kannan K, Ortmann RA, and Fang D (2008) Synoviolin promotes IRE1 ubiquitination and degradation in synovial fibroblasts from mice with collagen-induced arthritis. EMBO reports 9, 480–485 [PubMed: 18369366]
46. Yagishita N, Ohneda K, Amano T, Yamasaki S, Sugiura A, Tsuchimochi K, Shin H, Kawahara K, Ohneda O, Ohta T, Tanaka S, Yamamoto M, Maruyama I, Nishioka K, Fukamizu A, and Nakajima

T (2005) Essential role of synoviolin in embryogenesis. J Biol Chem 280, 7909–7916 [PubMed: 15611074]

47. Lobanova ES, Finkelstein S, Li J, Travis AM, Hao Y, Klingeborn M, Skiba NP, Deshaies RJ, and Arshavsky VY (2018) Increased proteasomal activity supports photoreceptor survival in inherited retinal degeneration. Nat Commun 9, 1738 [PubMed: 29712894]
48. Lobanova ES, Finkelstein S, Skiba NP, and Arshavsky VY (2013) Proteasome overload is a common stress factor in multiple forms of inherited retinal degeneration. Proc Natl Acad Sci U S A 110, 9986–9991 [PubMed: 23716657]
49. Yang S, He H, Ma QS, Zhang Y, Zhu Y, Wan X, Wang FW, Wang SS, Liu L, and Li B (2015) Experimental study of the protective effects of SYVN1 against diabetic retinopathy. Sci Rep 5, 14036 [PubMed: 26358086]
50. Baldridge WH, Kurennyi DE, and Barnes S (1998) Calcium-sensitive calcium influx in photoreceptor inner segments. J Neurophysiol 79, 3012–3018 [PubMed: 9636104]
51. Szikra T, Cusato K, Thoreson WB, Barabas P, Bartoletti TM, and Krizaj D (2008) Depletion of calcium stores regulates calcium influx and signal transmission in rod photoreceptors. J Physiol 586, 4859–4875 [PubMed: 18755743]
52. Ding XQ, Harry CS, Umino Y, Matveev AV, Fliesler SJ, and Barlow RB (2009) Impaired cone function and cone degeneration resulting from CNGB3 deficiency: down-regulation of CNGA3 biosynthesis as a potential mechanism. Hum Mol Genet 18, 4770–4780 [PubMed: 19767295]
53. Yorimitsu T, Nair U, Yang Z, and Klionsky DJ (2006) Endoplasmic reticulum stress triggers autophagy. J Biol Chem 281, 30299–30304 [PubMed: 16901900]

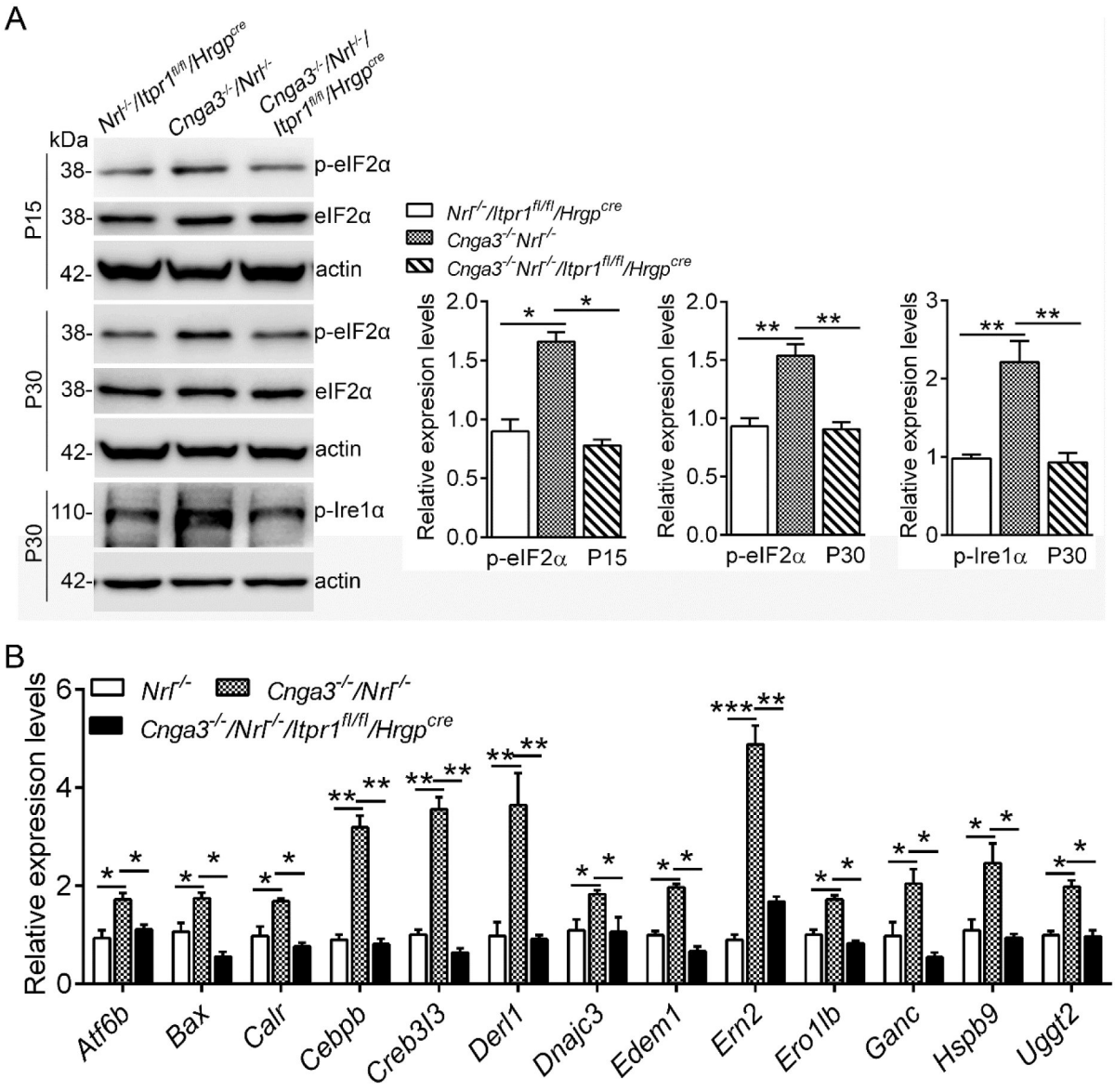

Figure 1. Deletion of IP_3R1 reduced UPR/ER stress in CNG channel-deficient retinas.

A. Expression levels of ER stress marker proteins in mouse retinas at P15 and P30 were analyzed by immunoblotting. Shown are representative immunoblotting images of these detections and corresponding quantitative analysis, following normalization to internal loading control β-actin. **B.** Expression of UPR genes was evaluated in mouse retinas at P15 by PCR array. Shown are PCR array results. Data are presented as mean ± *SEM* of 3–4 independent assays using retinas from 8–10 mice (*$p < 0.05$, **$p < 0.01$, ***$p < 0.001$).

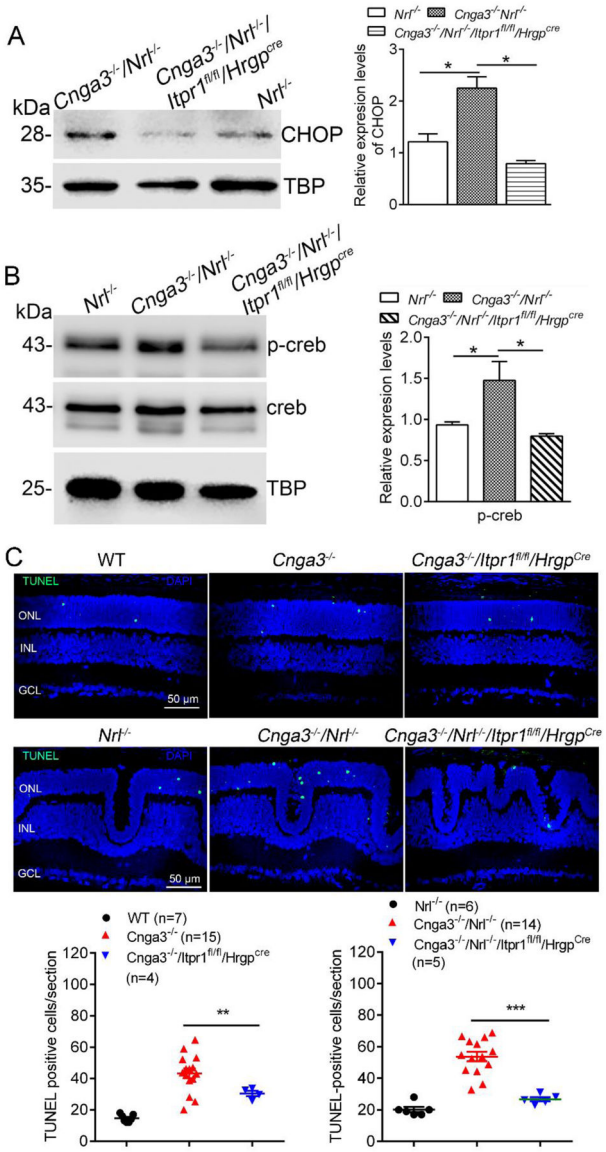

Figure 2. Deletion of IP_3R1 reduced ER stress downstream signaling and apoptosis in CNG channel-deficient retinas.

A-B. Expression of CHOP and p-Creb were evaluated in mouse retinas by immunoblotting. Shown are representative immunoblotting images for CHOP at P15 (**A**) and p-Creb at P30 (**B**) and the corresponding quantitative analysis. **C.** Photoreceptor apoptosis was evaluated by TUNEL labeling on retinal sections of CNG channel-deficient mice at P15. Shown are representative confocal images of TUNEL labeling and correlating quantitative analysis. ONL, outer nuclear layer; INL, inner nuclear layer. Data are presented as mean ± *SEM* of 3–4 independent assays using retinas/eye sections from 4–10 mice (*$p < 0.05$, **$p < 0.01$, ***$p < 0.001$).

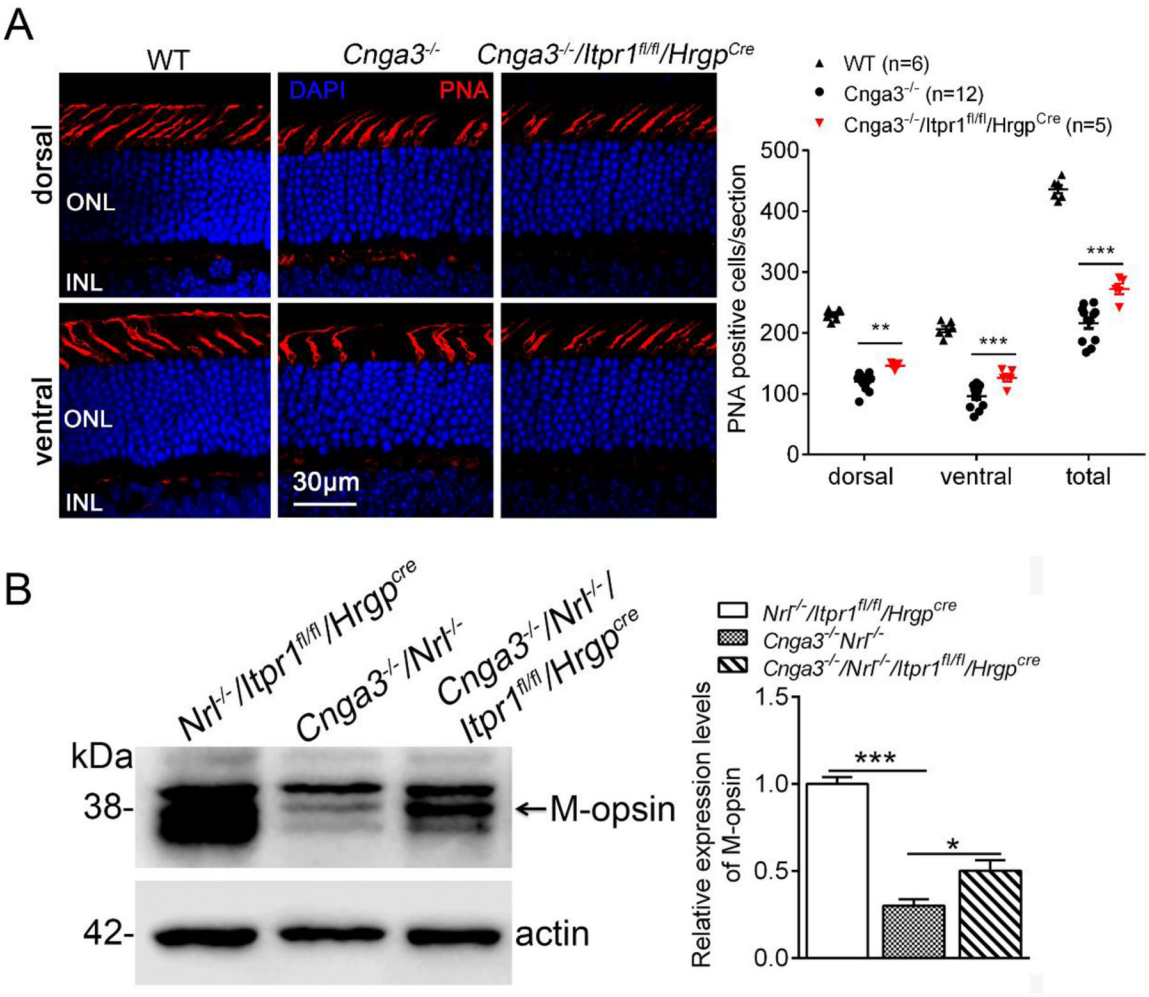

Figure 3. Deletion of IP_3R1 increased cone density and expression levels of M-opsin in CNG channel-deficient retinas.

A. Cone density was evaluated by PNA labeling on retinal sections prepared from mice at 2 months. Shown are representative confocal images of PNA labeling on retinal sections and corresponding quantitative analysis. ONL, outer nuclear layer. **B.** Expression levels of M-opsin were analyzed by immunoblotting at P30. Shown are representative immunoblotting images and the corresponding quantitative analysis. Data are presented as mean ± *SEM* of 3–4 independent assays using retinas/eye sections from 5–12 mice (**$p < 0.01$, ***$p < 0.001$).

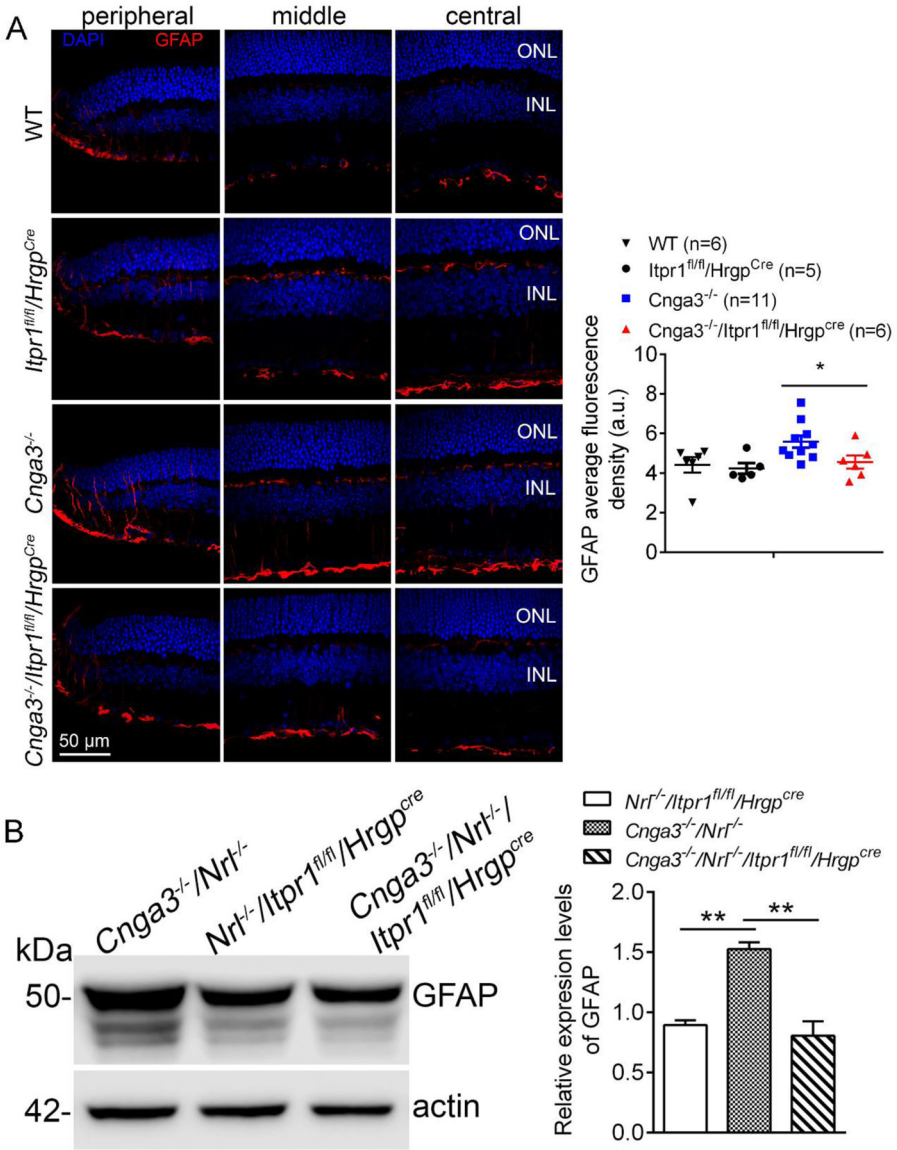

Figure 4. Deletion of IP_3R1 reduced activation of Müller glial cells in CNG channel-deficient retinas.

A. GFAP immunofluorescence labeling was performed on the retinal sections prepared from mouse eyes at P30. Shown are representative confocal images of immunofluorescence labeling of GFAP on the peripheral, middle, and central regions of the retinal sections and corresponding quantification of immunofluorescence intensity. ONL, outer nuclear layer; INL, inner nuclear layer; RGC, retinal ganglion cell. **B.** Expression levels of GFAP were evaluated in the mouse retinas by immunoblotting at P30. Shown are representative immunoblotting images of GFAP and corresponding quantitative analysis. Data are presented as mean ± *SEM* of 3–4 independent assays using retinas/eye sections from 5–12 mice (**$p < 0.01$).

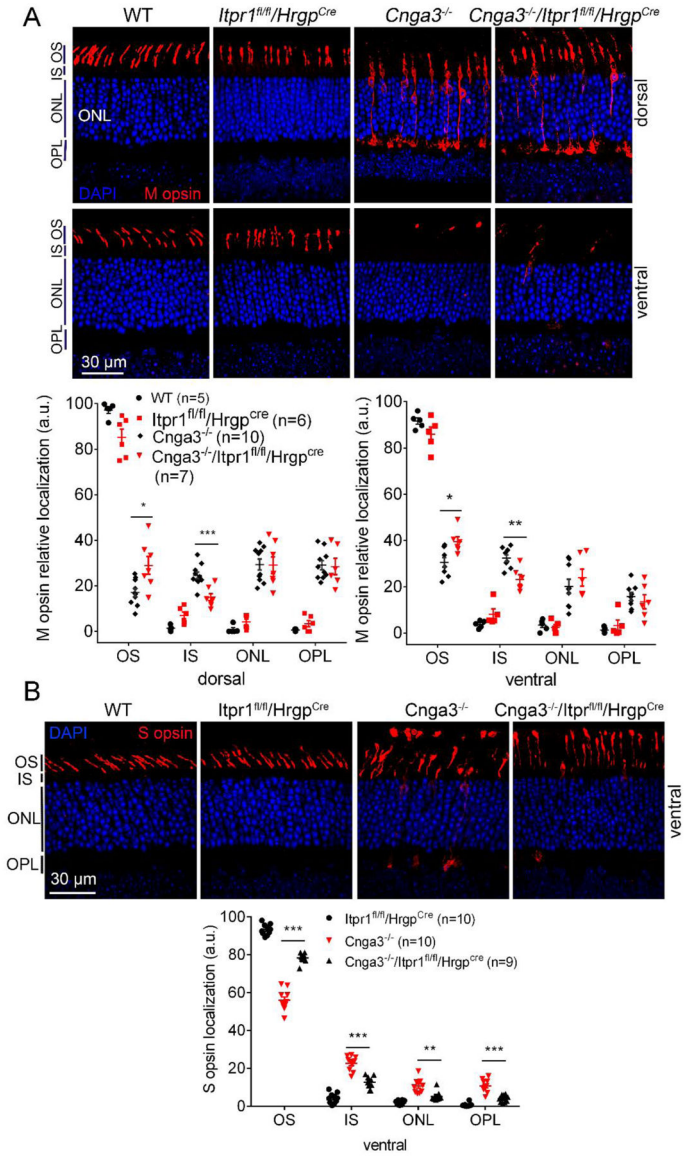

Figure 5. Deletion of IP_3R1 increased OS localization of cone opsin in CNG channel-deficient retinas.

M- and S-cone opsin localization were evaluated by immunofluorescence labeling on retinal cross sections prepared from mice at P30. Shown are representative confocal images of immunofluorescence labeling of M-opsin (**A**) and S-opsin (**B**) and corresponding quantitative analysis of immunofluorescence intensity level at different regions of the retinal cross sections. OS, outer segment; IS, inner segment; ONL, outer nuclear layer; OPL, outer plexiform layer. Data are presented as mean ± *SEM* of 3–4 independent assays using retinas/eye sections from 5–10 mice (*, $p < 0.05$; **, $p < 0.01$; ***, $p < 0.001$).

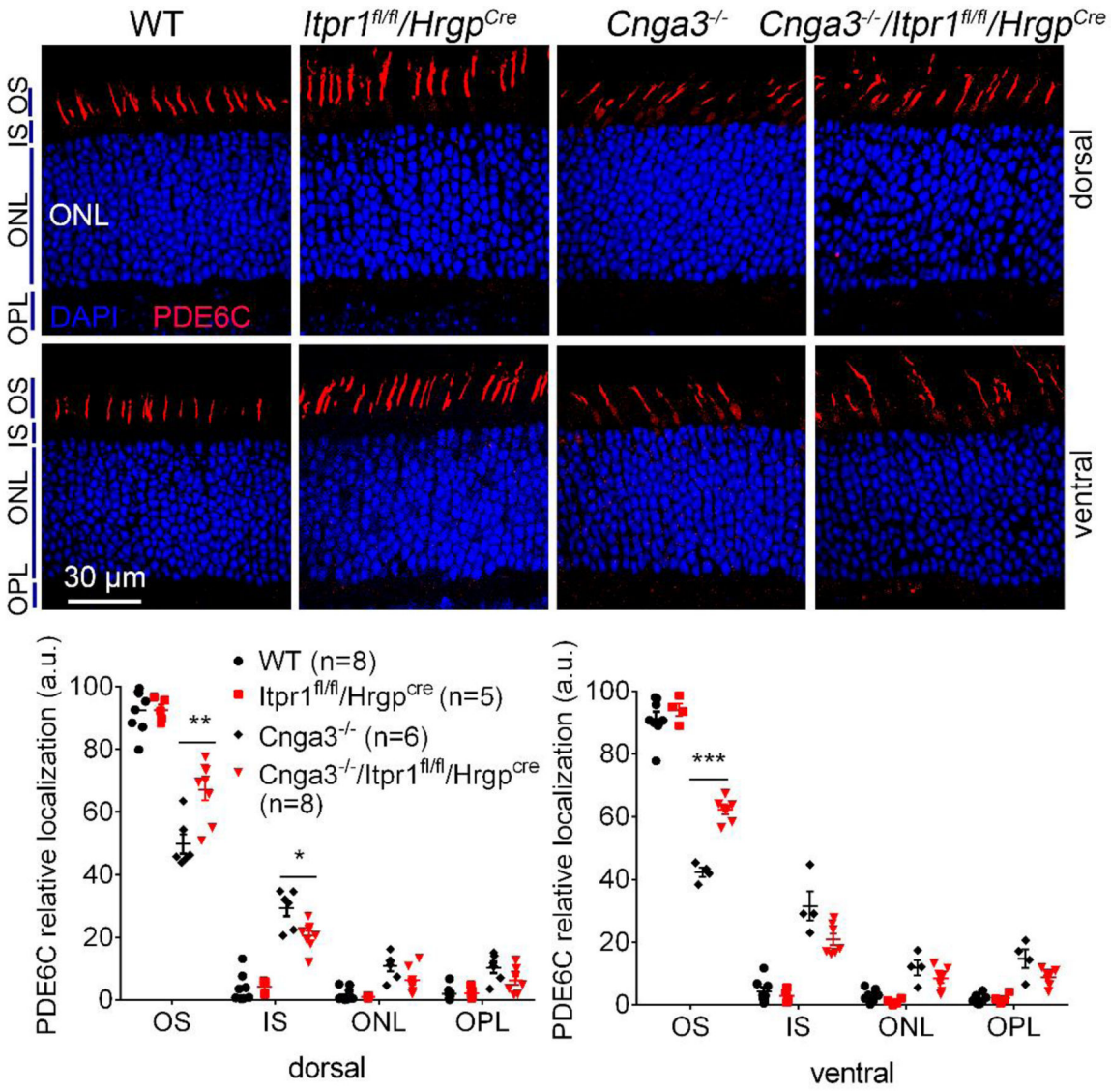

Figure 6. Deletion of IP_3R1 increased OS localization of PDE6C in CNG channel-deficient retinas.

PDE6C localization was evaluated by immunofluorescence labeling on retinal cross sections prepared from mice at P30. Shown are representative confocal images of immunofluorescence labeling of PDE6C (**A**) and corresponding quantitative analysis of immunofluorescence intensity level at different regions of the retinal cross sections (**B**). OS, outer segment; IS, inner segment; ONL, outer nuclear layer; OPL, outer plexiform layer. Data are presented as mean ± *SEM* of 3–4 independent assays using retinas/eye sections from 5–8 mice (*, $p < 0.05$; **, $p < 0.01$; ***, $p < 0.001$).

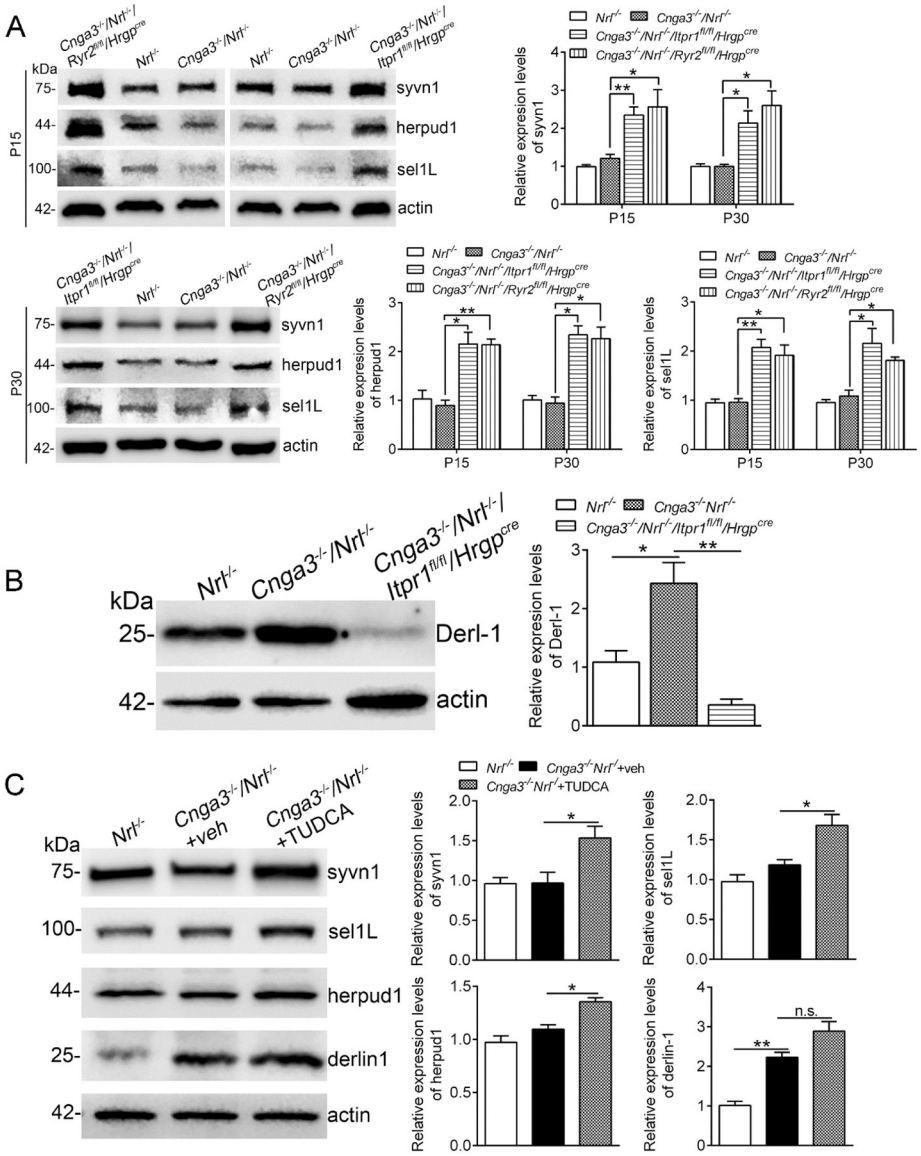

Figure 7. Deletion of IP_3R1 or treatment with TUDCA increased expression of ER retrotranslocation proteins in CNG channel-deficient retinas.

Expression levels of ER retrotranslocation proteins in mouse retinas at P15 and P30 (**A-B**), and after TUDCA treatment (**C**) were analyzed by immunoblotting. Shown are representative immunoblotting images of these detections and corresponding quantitative analysis, following normalization to internal loading control β-actin. Data are presented as mean ± *SEM* of 3–4 independent assays using retinas from 8–10 mice (*$p < 0.05$, **$p < 0.01$).

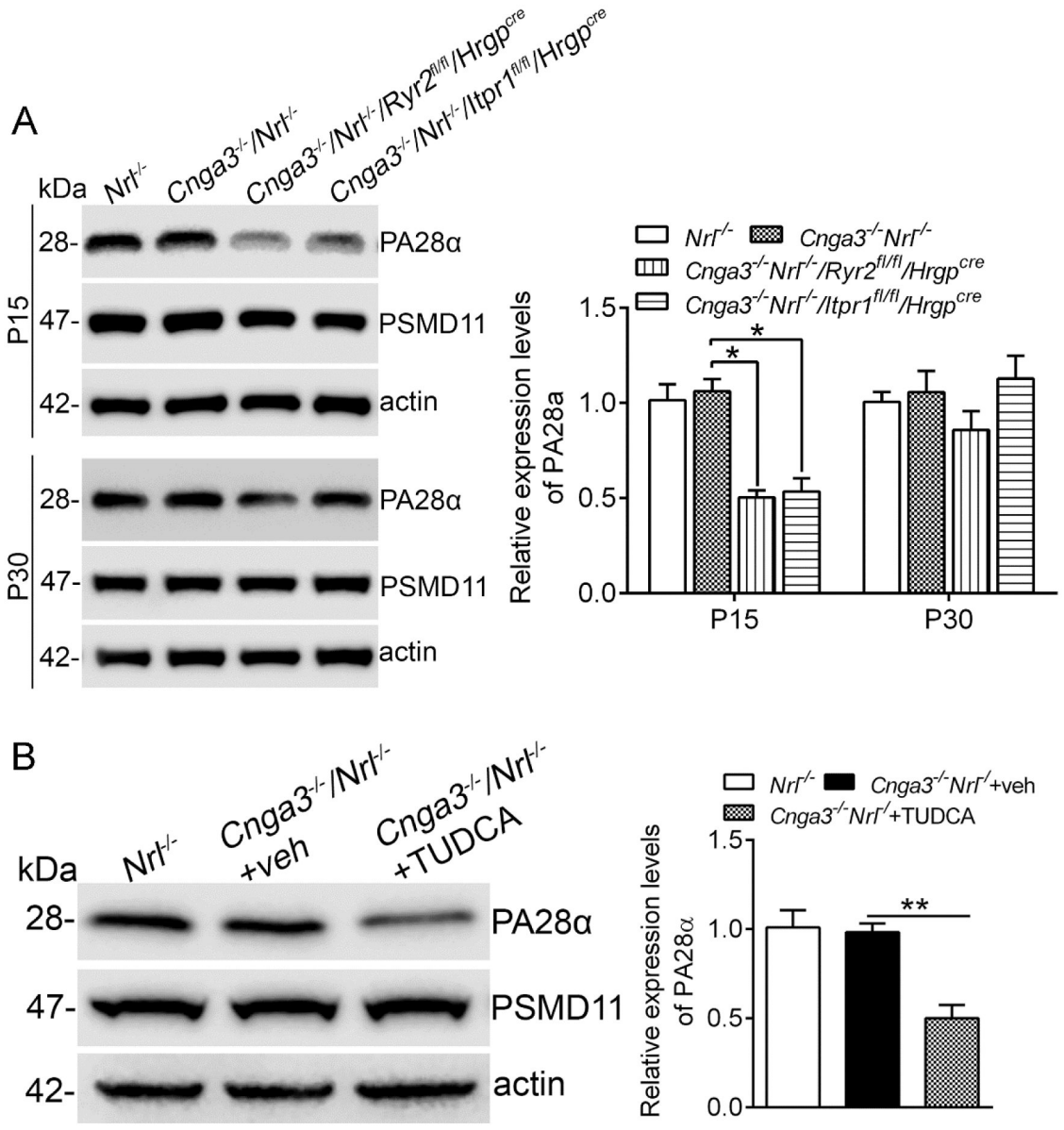

Figure 8. Deletion of IP_3R1 or treatment with TUDCA decreased expression of the proteasome subunit in CNG channel-deficient retinas.

Expression levels of the proteasome subunits in mouse retinas at P15 and P30 (**A**) and after TUDCA treatment (**B**) were analyzed by immunoblotting. Shown are representative immunoblotting images of these detections and corresponding quantitative analysis, following normalization to internal loading control β-actin. Data are presented as mean ± *SEM* of 3–4 independent assays using retinas from 8–10 mice (*$p < 0.05$, **$p < 0.01$).

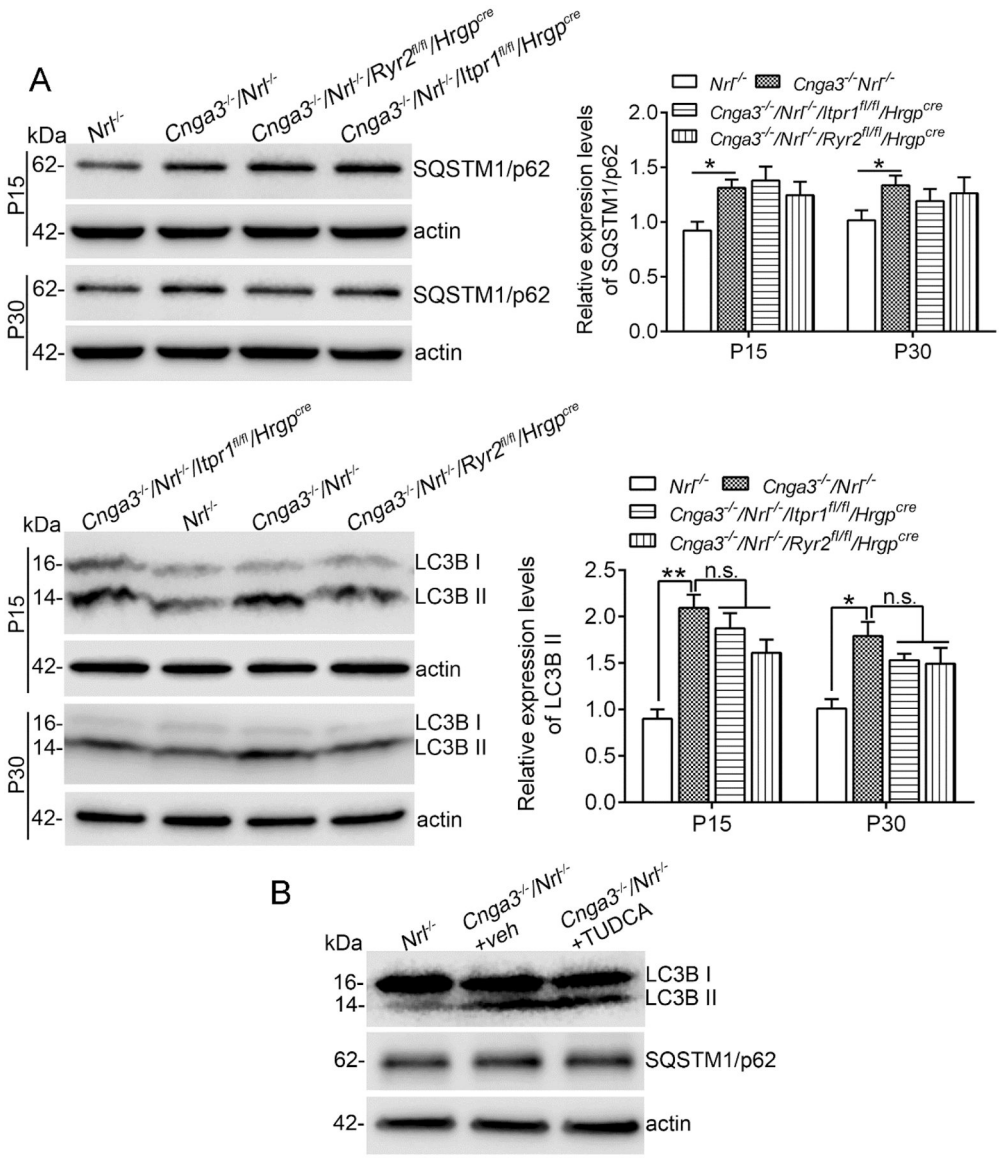

Figure 9. Deletion of IP_3R1 did not affect autophagy activity in CNG channel-deficient retinas.

Expression levels of autophagy marker proteins in mouse retinas (**A**) and after TUDCA treatment (**B**) were analyzed by immunoblotting. Shown are representative immunoblotting images of these detections and corresponding quantitative analysis, following normalization to internal loading control β-actin. Data are presented as mean ± *SEM* of 3–4 independent assays using retinas from 8–10 mice (*$p < 0.05$, **$p < 0.01$).

Table 1.

List of primary antibodies

Antibody	Provider	Catalog No.	Dilutions used in IB or IF
M-opsin	EMD Millipore	AB5405	1: 500 (IB) 1: 200 (IF)
S-opsin	Dr. Muna Naash from University of Houston		1: 200 (IF)
PDE6C	Abgent	AP9728	1: 200 (IF)
p-eIF2α	Cell signaling	3398	1: 500 (IB)
eIF2α	Cell signaling	9722	1: 500 (IB)
p-Ire1α	Abcam	ab48187	1: 500 (IB)
p-creb	Cell signaling	91985	1: 500 (IB)
Creb	Cell signaling	9197	1: 500 (IB)
GFAP	Dako	Z0334	1: 500 (IB) 1: 500 (IF)
Derl-1	Abcam	ab176732	1: 500 (IB)
Syvn1	Proteintech	13473–1-AP	1: 500 (IB)
Sel1L	LSBio	LS-C747272	1: 500 (IB)
Herpud1	Thermo Fisher Scientific	PA5–29469	1: 500 (IB)
PA28α	Cell signaling	2408	1: 500 (IB)
PSMD11	Cell signaling	14303	1: 500 (IB)
CHOP	Cell signaling	2985	1: 500 (IB)
TBP	Thermo Fisher Scientific	MA1–10883	1: 1000 (IB)
β-actin	Abcam	ab6276	1: 2000 (IB)
SQSTM1/p62	Cell signaling	5114	1: 500 (IB)
LC3B	Cell signaling	2775	1: 500 (IB)